LAWRENCE
LIVERMORE
NATIONAL
LABORATORY

LLNL-JRNL-611992

X-ray Thomson scattering measurements of temperature and density from multi-shocked CH capsules

L. B. Fletcher, S. H. Glenzer, A. Kritcher, A. Pak, T. Ma, T. Doeppner, C. Fortmann, L. Divol, O. L. Landen, J. Vorberger, D. Chapman, D. Gericke, R. W. Falcone

January 22, 2013

Physics of Plasmas

Disclaimer

X-ray Thomson scattering measurements of temperature and density from multi-shocked CH capsules

L. B. Fletcher[1*], A. Kritcher[3], A. Pak[3], T. Ma[3], T. Döppner[3], C. Fortmann[3,4], L. Divol[3], O.L. Landen[3], J. Vorberger[5], D. Chapman[5], D. Gericke[5], R.W. Falcone[1,2], and S.H. Glenzer[3]

[1]*University of California, Berkeley, CA 94720, USA*

[2]*Lawrence Berkeley National Laboratory, Berkeley, CA 94720, USA*

[3]*Lawrence Livermore National Laboratory, 7000 East Av., Livermore, CA 94550, USA*

[4]*University of California, Los Angeles, CA 90095, USA*

[5]*Centre for Fusion, Space and Astrophysics, University of Warwick, UK*

Proof-of-principle measurements of the electron densities, temperatures, and ionization states of spherically compressed multi-shocked CH (polystyrene) capsules have been achieved using spectrally resolved x-ray Thomson scattering. A total of 13.5 kJ incident on a CH shell, are used to compress a 70 μm thick CH shell above solid-mass density using three coalescing shocks. Separately, a laser-produced Zinc He-α x-ray source at 9 keV delayed 200 ps - 800 ps in time after maximum compression is used to probe the plasma in the non-collective scattering regime. The data show that x-ray Thomson scattering enables a complete description of the time-dependent hydrodynamic evolution of shock-compressed CH capsules, with a maximum measured compression of $\rho > 6$ g cm^{-3}. In addition, the results demonstrate that accurate measurements of x-ray scattering from bound-free transitions in the CH plasma demonstrate strong evidence that continuum lowering is the primary ionization mechanism of carbon L-shell electrons.

I. INTRODUCTION

Understanding the nature of warm dense matter (WDM) is of considerable practical importance to many areas of high-energy physics. WDM occupies conditions between the physical regimes of condensed matter and weakly coupled plasmas where material densities are typically on the order of 0.1-10 times solid density and temperatures are between 0.1 to 100 eV. It is in this non-ideal regime where simple approximations break down and a complete theoretical description of the state of matter becomes increasingly difficult. Such extreme conditions are not only common in astrophysical environments and believed to exist in the inner core of large planets (e.g., Jupiter or Saturn) [1-3], but also exist during laser and ion beam heating of materials [4], along with the first stages of compression in inertial confinement fusion (ICF) experiments [5, 6]. Thus, accurate modeling of matter at extreme conditions is of central interest in designing and understanding fusion energy experiments that are currently taking place at the National Ignition Facility [7, 8].

A. Coalescing shocks

Single shock pressures on the order of 20-40 Mbar have been achieved by direct, high-intensity laser irradiation of a low-Z ablator surface, such as a CH foil [9-15]. However, single shocks can only create states along the single-shock Hugoniot [16]. Laser pulse shaping can be used to generate a sequence of multiple, time-delayed shocks. These separate shocks, controlled by the laser intensity and pulse duration, can be used to compress a sample nearly isentropically

resulting in pressures beyond 100 Mbar at relatively low temperatures (T_e < 15 eV). Figure 1 shows the ability to use three coalescing shocks to exceed previously measured single shock Hugoniot equation of state (EOS) results for shock-compressed CH capsules, thus providing an excellent method to evaluate and benchmark current computational hydrodynamics models in the high-energy regime. In this paper, we present an experimental platform that can spherically compress CH capsules with solid densities up to 8 g/cc exceeding 100 Mbar in pressure using multiple coalescing shocks, while simultaneously measuring the electron temperatures and electron densities using spectrally resolved x-ray Thomson scattering [17-24]. By directly measuring the mass density, electron temperature, and the ionization state, it is possible to observe the dynamic behavior of the plasma in order to verify compression using three shocks and understand the hydrodynamic evolution of coalescing shocks in imploding CH capsules.

B. X-ray Thomson scattering

X-ray Thomson scattering has proven to be an accurate *in situ* diagnostic tool that can be used to determine the properties of above solid-density plasmas [17]. X-ray Thomson scattering is the scattering of x-ray radiation by electrons in a material that are either free, weekly bound, or tightly bound to the ion. The total scattered x-ray spectrum demonstrates a unique intensity profile and spectral shape that depends on a combination of scattering contributions that are distinctly related to the temperature, density, and ionization state of the plasma [26]. The total scattered cross section (Equation 1) can be described in terms of σ_T, the Thomson scattering cross-section, and k_1 and k_o, the scattered and incident wave vectors, respectively.

$$\frac{\partial^2 \sigma_T}{\partial \Omega \partial \omega} = \sigma_T \frac{k_1}{k_o} S(k,\omega) \tag{1}$$

It is possible to separate the total density fluctuations between the free Z_f, and bound Z_b electron contributions, as well as the motion of the ions. The details of this procedure are given by Chihara [26, 27], where the probability of finding ions and electrons with respect to other ions and electrons in the plasma is expressed by the total dynamic structure factor S(k,ω), which can be described by the following Equation.

$$S(k,\omega) = \left|f_1(k) + q(k)\right|^2 S_{ii}(k,\omega) + Z_f S^o_{ee}(k,\omega) + Z_b \int S_{ce}(k,\omega - \omega') S_s(k,\omega') \partial\omega' \tag{2}$$

The first term in Equation 2 results from elastic scattering of tightly bound electrons (Rayleigh scatter) that are co-moving with the ions where $f_i(k)$ is the atomic form factor describing the elastic scattering from bound electrons, q(k) contains the contribution from the electrons in the screening cloud around the ion [28], and $S_{ii}(k)$ is the ion-ion density correlation function.

The second term in Equation 2 describes the inelastic scattering due to free electrons, where $S_{ee}(k,\omega)$ is the electron-electron density correlation function and Z_f is the effective free ionization state. For relatively low temperatures and high densities produced by the coalescing shock waves, the plasma is expected to be weakly degenerate [24]. Under such conditions, the width of the inelastic scatter is sensitive to changes in the Fermi energy E_F and can be used to calculate the electron density, n_e. The shape of the Compton signal can also be used to infer information on the electron temperature, T_e.

The third term in Equation 2 describes inelastic excitations of states within an atom or ion into the continuum, represented by $S_{ce}(k, \omega)$ where Z_b is the effective bound ionization state. Such scattering from these weakly bound states will demonstrate a Compton shift where the incident x-ray photons can transfer their energy to the electrons [29]. Such bound-free transitions are modulated by the self-motion of the ion, $S_s(k, \omega)$. This entire contribution has been neglected, or treated as a background constant in many previous low-Z experiments [18-21]. However, for relatively higher Z materials, such as carbon, this scattering component can demonstrate a significant contribution [30, 31]. In addition, weak scatter from bound electrons spectrally shifted beyond the inelastic scattered signal can be used to calculate the ionization state of the CH via the relative ratio of the measured bound-free to free-free (inelastic) signals. By spectrally resolving the scattering, the elastic unshifted scattering component can be separated from these bound-free transitions, along with the Compton shifted inelastic component.

The theoretical screening formalism for the expected elastic x-ray Thomson scattered signals in a multi-component plasma, such as CH, are typically calculated using a weighted average for carbon and hydrogen, where carbon demonstrates the largest contribution [32]. The Debye limit for the carbon screening function $q_C(k)$ is approximated by the following Equation.

$$q(k) \approx \frac{Z^* \kappa^2}{k^2 + \kappa^2} \tag{3}$$

However, this approximation is only valid for small k. Under many experimental conditions, the Debye approximation is sufficient as the k-value probed is either in this limit, or the value q(k) is insignificant for large k ($q \sim 0$) as the screening function is itself negligible (Figure 2). In this experiment, we are probing the plasma in an intermediate regime where the standard Debye

approximation needs to be replaced with a more accurate solution, such as the full random phase approximation (RPA) [32, 33], where the screening function q(k) is not yet negligible. Thus, one can expect ~16% reduction in the elastic scattering contribution as calculated with the Debye approximation. This discrepancy can clearly be observed at $k*a_B=4.445$, as probed, and is the first time such an effect has been important when calculating accurate measurements of the electron temperature via the absolute intensity of the Rayleigh scattering contribution.

C. Continuum lowering

In the case of highly compressed states of matter, the electric field distribution of an ion can be influenced by its own bound electrons as well as the field of neighboring ions. Such a situation can result in ionization potential depression (i.e. continuum lowering). The amount by which the continuum is depressed can be calculated by the change in the energy of the electrostatic potential produced by the ionization of an ion. Modification to the potential around the ion is a function of the screening distance of the Coulomb forces and the number of ions that participate in the processes [34-36]. However, a solution to such a complex multi-body problem is not trivial. There are many different models (or combination of models) that can be used to calculate the net lowering of the ionization potential. Models such as the Stewart–Pyatt, Ecker-Kroll, Debye–Huckel, or the ion-sphere average atom approach all depend on different assumptions in the charge screening calculations [37-39]. Due to the difficulties of creating states of matter, with a known density, that are extremely dense and ionized at the same time, many of these models have not been systematically evaluated. However, recent results from Ciricosta *et al*. [40] have renewed an interest in this topic and have called attention to the accuracy of these different

models. X-ray Thomson scattering from bound-free transitions provides information about the level of continuum lowering under well-characterized n_e and T_e plasma conditions. For many high-energy density experiments, the predicted ΔE can account for approximately 10–40 % of the ionization energy, depending on the continuum lowering model used and the plasma conditions created. L-shell edges in carbon are within this energy range, thus the contribution of x-ray scattering from bound-free L-shell electrons can be used to accurately monitor any additional ionization that is caused by continuum lowering.

II. EXPERIMENT

In this experiment, empty CH capsules, 70 μm thick were isotropically irradiated using 13.5 kJ of 351 nm (3ω) ultraviolet laser light. We then probed the compressed plasma interior using a high-energy Zinc He-α x-ray source at 9 keV from a separate laser irradiated Zinc foil. Figure 3a shows a schematic of the experimental configuration and the target geometry along with a photograph of the target (Fig. 3b). In addition, hydrodynamic simulations performed with Helios (Fig. 3c) demonstrate the possibility of compressing 70 μm thick CH ablators up to 8 g cm^{-3} using three co-propagating coalescing shocks [41]. The simulations show that a mass density of approximately 7x the initial solid-density (ρ_{CH}=1.1 g cm^{-3}) can be accomplished using a pulse shape, shown in Figure 3c lineout, with three timed steps of 1 ns, 1.5 ns, and 500 ps in time duration along with precisely controlled amplitudes of 0.67 TW, 6.85 TW, and 15.5 TW, respectively. Figure 3c shows the measured radii of the CH shell superimposed on radiation-hydrodynamic simulations of the shell mass density as function of time and shell radius. In the Figure, t = 0 ns indicates the start of the drive beams, and t = 3 ns is when the laser pulse has

turned off. The simulations predict peak compression (full shock coalescence) at the end of the 3 ns-long laser drive, after which the shock begins to dissipate.

Under a non-collective scattering geometry, using a scattering angle of θ=135° from the incident x-rays, a HOPG crystal spectrometer was used to spectrally resolve Thomson scattering signals using an energy range of approximately 7.4 to 11.8 keV, with a central energy of 9.6 keV, when operated in first order. Temporal resolution was achieved by probing the plasma using a time delay between the drive laser beams (used to heat the CH capsule) and the probe laser beams incident on a Zn foil (used to produce 9 keV Zinc He-α x-rays) in combination with a time-gated micro-channel plate (MCP) detector as part of the spectrometer setup.

III. RESULTS

The plasma generated in this experiment is weakly degenerate, as a result $T_e \sim T_F$ and the width of the inelastic scattering feature is only weakly sensitive to the electron temperature. However, as described previously, the inelastic scattering is strongly correlated with the electron density. The elastic scattering in contrast, is sensitive to the electron temperature and ionization, and is weakly correlated with the electron density. Therefore, the electron temperature can be constrained by the amount of Rayleigh scatter. By combining the theory outline in previous sections concerning the unique state of carbon L-shell bound-free transitions with the full RPA description for the elastic (Rayleigh) response, the best fits to theoretical spectra shown in Figure 4 allow one to infer the temperature, electron density, and ionization state of shock compressed CH as a function of time.

Results in Figure 4 shows the time ordered sequence of the spectrally resolved x-ray

Thomson scattering signals, where the earliest x-ray scattering spectrum is collected 400 ps after expected peak compression. Figure 4 demonstrates an elastic scattering component, measured at ~9 keV, and a down-shifted inelastic Compton feature at ~8.75 keV. From the Figure one can notice that the inelastic scatter is shifted by the expected Compton energy of E_C = 245 eV and is spectrally broadened. The changing shape of the Compton feature with respect to time, as seen in Figure 4, shows that the electron density and the electron temperature change with shock propagation. The Compton feature at each time of 3.4 ns, 3.5 ns, 3.6 ns, and 3.8 ns represent the response of the compressed state during shock coalescence. The synthetic x-ray Thomson scattering spectrum best theoretical fit of the electron velocity distribution to the experimental data yields a systematic decrease in both the electron temperature T_e of = 10 eV, 8 eV, 6 eV, 6 eV and the electron density n_e = 1.40 x 10^{24} cm^{-3}, 1.05 x 10^{24} cm^{-3}, 0.95 x 10^{24} cm^{-3}, 0.80 x 10^{24} cm^{-3} with respect to time.

By directly comparing the measured scattered spectra to the calculated total dynamic structure factor, we can accurately determine the n_e and T_e of the plasma. In Figure 5, the statistical differences between the theoretical fits to the measured experimental data at 3.4 ns, as calculated by the root mean squared (RMS), demonstrates contour lines for the RMS as a function of n_e and T_e. As mentioned previously, the electron density is calculated from first principles, the electron temperature uses a combination models that are reflected in the entire scattered profile. This fitting technique allows for the ability to measure a unique combination of both the electron density and temperature simultaneously from the shape of the Compton profile and the absolute intensity of the elastic scattering feature. The global minimum as defined by the minimum innermost contour, in Figure 5, indicates the range of best fits to the experimental data that correspond to the best-fit theoretical curve, shown in Figure 4. This global minimum can be

used to characterize a well-defined range of uncertainties in our final analysis. From our analysis, sensitivity of experimental fitting to both the inelastic and the elastic scattering features can be as low as 10 % error for n_e and 15 % error in T_e.

Profiles of the bound-free dynamic structure factor for carbon plasmas, for two different bound-free models Impulse Approximation (IA) and Form Factor Approximation (FFA), at different ionization states of Z_C=2, and Z_C=4 are demonstrated in Figure 6. FFA is calculated by using the first Born approximation and hydrogenic wavefunctions for both the initial and final states of the core electron [42]. A more comprehensive treatment of the core electrons using IA assumes that the ionization potential depression is close to the ionization energy of the L-shell electron, effectively the electron is nearly free and the bound scattering contribution should look very similar to the free one resulting in a shift in energy that is on the same scale as Compton feature [43, 44]. The valence L-shell electrons of carbon are highly localized in momentum space and will result in a very narrow spectral band contribution to the Compton profile. The unique profile that results from the L-shell transition can be used to accurately determine the ionization state of the CH capsule for our conditions. It is clear from the profiles demonstrated in Figure 6 that there is no observable L-shell contribution to the total x-ray scatter in either bound-free approximation. Such a result indicates a complete depletion the L-shell electrons from which we can deduce a carbon ionization Z_C=4. In addition, it can be inferred from the measured electron temperatures that the hydrogen is fully ionized in this experiment (i.e. hydrogen ionization state Z_H=1). It should be noted, on the other hand, that plasma temperatures of T_e=10 eV are not high enough to result in a measured ionization state Z_C=4. Therefore other ionization mechanism, such as continuum lowering, may have a significantly large contribution to the observed ionization state of carbon. The results from this study are consistent with the earlier findings

presented by Ciricosta *et al*. [40] that demonstrate a larger than predicted ionization potential depression as calculated by many other widely used ionization models, such as Stewart-Pyatt (SP) and Ion-Sphere (IS). Using a measured carbon ionization state of Z_C=4 (with Z_H=1), results in a measured compression of 5.5x, 4.13x, 3.74x, 3.14x the solid mass density over this same time interval.

The time evolution of the electron temperature, electron density, and mass density of spherically shocked-compressed CH capsules can be observed in Figure 7. The results, in combination with the hydrodynamics simulation (HYDRA), demonstrate the ability to laser compress CH capsules to a peak condition of approximately 7x the initial solid-state density (Fig 7a). The measurements of the mass density (calculated via the ionization state) and electron temperature (Fig 7b) are in agreement with the hydrodynamics code, and do not demonstrate any significant deviation outside of the experimental error. However, the measured electron density (Fig 7c) deviates significantly from the predicted values. It is important to note that only at high ionization states (Z_C=4) will the results agree with the mass density as predicted by the hydrodynamic models. Due to the lack of L-shell contributions to the bound-free scatter and the low contribution of K-shell electrons, it is not possible to accurately discriminate between the two bound-free models IA and FFA when comparing the calculated plasma properties. Improved resolution using coherent x-ray lasers, where it is possible to take advantage of a high intensity and small bandwidth source, can greatly enhance our signal to noise as well as increase the separation between scattering components allowing for more accurate characterization of the bound-free models. Such high-precision measurements will be conceder in future investigations.

IV. CONCLUSIONS

We have successfully demonstrated the ability to measure ionization, compression, and heating of three coalescing shocks in CH capsules using Zn He-α x-ray Thomson scattering. Time resolved measurements of both the elastic and inelastic scatter have been used to examine the changes in both the electron temperature and the electron densities. In addition, we have successfully investigated the sensitivity in the bound-free scattering contribution and used the results to accurately determine the ionization state of shock-compressed carbon. To this end, there is strong evidence that continuum lowering is the primary ionization mechanism where only one unique solution, at high ionization states (Z_C=4), has demonstrated agreement with the theoretical x-ray Thomson scattered spectra using two different bound-free models. The presented results have important applications towards inertial confinement fusion experiments and highlight the importance towards accurate continuum lowering models or opacity tables for future implosion designs.

ACKNOWLEDGMENTS

This work was performed by the assistance of Lawrence Livermore National Laboratory (LLNL) under Contract DE-AC52-07NA27344 and supported by Laboratory Directed Research and Development (LDRD) grant 11-ER-050. Acknowledgements also extend to financial support by National Laser Users' Facility (NLUF) Grants: DE-FG52-07 NA28057 & DE-DE-FG52-09 NA29035.

REFERENCES

[1] T. Guillot, Science, 286, 72 (1999).

[2] B. A. Remington, P. R. Drake, and D. D. Ryutov, Rev. Mod. Phys. 78, 755 (2006).

[3] H. M. Van Horn, Science, 252, 384 (1991).

[4] M. Koenig, A. Benuzzi-Mounaix, A. Ravasio, T. Vinci, N. Ozaki, S. Lepape, D. Batani, G. Huser, T. Hall, D. Hicks, A. MacKinnon, P. Patel, H. S. Park, T. Boehly, M. Borghesi, S. Kar and L. Romagnani, Plasma Phys. Contr. Fusion 47, B441 (2005).

[5] J. D. Lindl, Inertial Confinement Fusion, Springer-Verlag, New York, 1998.

[6] S. Atzeni and J. Meyer-ter-Vehn, The Physics of Inertial Fusion, Clarendon Press, Oxford, 2004.

[7] S. H. Glenzer, D. A. Callahan, A. J. MacKinnon, J. L. Kline, G. Grim, E. T. Alger, R. L. Berger, L. A. Bernstein, R. Betti, D. L. Bleuel, T. R. Boehly, D. K. Bradley, S. C. Burkhart, R. Burr1, J. A. Caggiano, C. Castro, D. T. Casey4, C. Choate, D. S. Clark, P. Celliers, C. J. Cerjan, G. W. Collins, E. L. Dewald, P. DiNicola, J. M. DiNicola, L. Divol, S. Dixit, T. Döppner, R. Dylla-Spears, E. Dzenitis, M. Eckart, G. Erbert, D. Farley, J. Fair, D. Fittinghoff, M. Frank, L. J. A. Frenje, S. Friedrich, D. T. Casey, M. Gatu Johnson, C. Gibson, E. Giraldez, V. Glebov, S. Glenn, N. Guler, S. W. Haan, B. J. Haid, B. A. Hammel, A. V. Hamza, C. A. Haynam, G. M. Heestand, M. Hermann, H. W. Hermann1, D. G. Hicks1, D. E. Hinkel, J. P. Holder, D. M. Holunda, J. B. Horner, W. W. Hsing, H. Huang, N. Izumi, M. Jackson, O. S. Jones, D. H. Kalantar, R. Kauffman, J. D. Kilkenny, R. K. Kirkwood, J. Klingmann, T. Kohut, J. P. Knauer, J. A. Koch, B. Kozioziemki, G. A. Kyrala, A. L. Kritcher, J. Kroll, K. La Fortune, L. Lagin, O. L. Landen, D. W. Larson, D. LaTray, R. J. Leeper, S. Le Pape, J. D. Lindl, R. Lowe-Webb, T. Ma, J. McNaney, A. G. MacPhee, T. N. Malsbury, E. Mapoles, C. D. Marshall, N. B. Meezan, F. Merrill, P. Michel, J. D. Moody, A. S. Moore, M. Moran, K. A. Moreno, D. H. Munro, B. R. Nathan, A. Nikroo, R. E. Olson, C. D. Orth, A. E. Pak, P. K. Patel, T. Parham, R. Petrasso, J. E. Ralph, H. Rinderknecht, S. P. Regan, H. F. Robey, J. S. Ross, M. D. Rosen, R. Sacks, J. D. Salmonson, R. Saunders, J. Sater, C. Sangster, M. B. Schneider, F. H. Séguin, M. J. Shaw, B. K. Spears, P. T. Springer, W. Stoeffl, L. J. Suter, C. A. Thomas, R. Tommasini, R. P. J. Town, C. Walters, S. Weaver, S. V. Weber, P. J. Wegner, P. K. Whitman, K. Widmann, C. C. Widmayer, C. H. Wilde, D. C. Wilson, B. [8] Van Wonterghem, B. J. MacGowan, L. J. Atherton, M. J. Edwards, and E. I. Moses, Phys. Plasmas 19, 056318 (2012).

[8] S.W. Haan, P.A. Amendt, T.R. Dittrich, B.A. Hammel, S.P. Hatchett, M.C. Herrmann, O.A. Hurricane, O.S. Jones, J.D. Lindl, M.M. Marinak, D. Munro, S.M. Pollaine, J.D. Salmonson, G.L. Strobel1 and L.J. Suter, Nucl. Fusion 44, S171 (2004).

[9] I. P. Dudoladov, V. I. Rakitin, Y. N. Sutulov, G. S. Telegin, J. of App. Mech. and Tech. Phys., 10, 4 (1969).

[10] R. G. McQueen, S. P. Marsh, J. W. Taylor, High Velocity Impact Phenomena, Academic, New York, 1970.

[11] S. P. Marsh , LASL Shock Hugoniot Data, Los Alamos Series on Dynamic Material Properties, University of California Press, Berkeley, 1980.

[12] A. V. Bushman, I. V. Lomonosov, V. E. Fortov, and K. V. Khishchenko, JETP Lett. 82, 895 (1996).

[13] M. Van Thiel, J. Shaner, and E. Salinas, Lawrence Livermore National Laboratory Report No. UCRL-50108, 1977.

[14] R. Cauble, T. S. Perry, D. R. Bach, K. S. Budil, B. A. Hammel, G. W. Collins, D. M. Gold, J. Dunn, P. Celliers, L. B. Da Silva, M. E. Foord, R. J. Wallace, R. E. Stewart, and N. C. Woolsey, Phys. Rev. Lett. 80, 1248 (1998).

[15] N. Ozaki, T. Ono, K. Takamatsu, K. A. Tanaka, M. Nakano, T. Kataoka, M. Yoshida, K. Wakabayashi, M. Nakai, K. Nagai, K. Shigemori, T. Yamanaka, and K. Kondo, Phys. Plasmas 12, 124503 (2005).

[16] Y. Zel'Dovich and Y. Raizer, in Physics of Shock Waves and High-Temperature Hydrodynamic Phenomena, edited by W. D. Hayes and R. F. Probstein, Dover, Mineola, NY, 2002.

[17] S. H. Glenzer and R. Redmer, Rev. Mod. Phys. 81, 1625 (2009).

[18] S. H. Glenzer, G. Gregori, R. W. Lee, E. J. Rogers, S. W. Pollaine, and O. L. Landen, Phys. Rev. Lett., 90,175002 (2003).

[19] S. H. Glenzer, G. Gregori, E. J. Rogers, D. H. Froula, S. W. Pollaine, R. S. Wallace, and O. L. Landen, Phys. Plasmas, 10, 2433 (2003).

[20] S. H. Glenzer, O. L. Landen, P. Neumayer, R. W. Lee, K. Widmann, S. W. Pollaine, R. J. Wallace, G. Gregori, A. Höll, T. Bornath, R. Thiele, V. Schwarz, W.-D. Kraeft, and R. Redmer, Phys. Rev. Lett. 98, 065002 (2007).

[21] A. L. Kritcher, T. Döppner, C. Fortmann, T. Ma, O. L. Landen, R. Wallace, and S. H. Glenzer, Phys. Rev. Lett. 107, 015002 (2011).

[22] B. Barbrel, M. Koenig, A. Benuzzi-Mounaix, E. Brambrink, C. R. D. Brown, D. O. Gericke, B. Nagler, M. Rabec le Gloahec, D. Riley, C. Spindloe, S. M. Vinko, J. Vorberger, J. Wark, K. Wünsch, and G. Gregori, Phys. Rev. Lett. 102, 165004 (2009).

[23] H. J. Lee, P. Neumayer, J. Castor, T. Döppner, R. W. Falcone, C. Fortmann, B. A. Hammel, A. L. Kritcher, O. L. Landen, R. W. Lee, D. D. Meyerhofer, D. H. Munro, R. Redmer, S. P. Regan, S. Weber, and S. H. Glenzer, Phys. Rev. Lett. 102, 115001 (2009).

[24] O. L. Landen, O. L., S. H. Glenzer, M. J. Edwards, R. W. Lee, G. W. Collins, R. C. Cauble, W. W. Hsing, and B. A. Hammel, J. Quant. Spectrosc. Radiat. Transf. 71, 465 (2001).

[25] G. Gregori, S. H. Glenzer, W. Rozmus, R. W. Lee, and O. L. Landen, Phys. Rev. E, 67, 026412 (2003).

[26] J. Chihara, J. Phys. F: Met. Phys. 17, 295 (1987).

[27] J. Chihara, J. Phys. : Condens. Matter 12, 231 (2000).

[28] D. Riley, N. C. Woolsey, D. McSherry, I. Weaver, A. Djaoui, and E. Nardi, Phys. Rev. Lett., 84, 1704 (2000).

[29] G. Gregori, S. H. Glenzer, F. J. Rogers, S. M. Pollaine, O. L. Landen, C. Blancard, G. Faussurier, P. Renaudin, S. Kuhlbrodt, and R. Redmer, Phys. Plasmas 11, 2754 (2004).

[30] G. Gregori, S. Glenzer, H. Chung, D. Froula, R. Lee, N. Meezan, J. Moody, C. Niemann, O. Landen, B. Holst, R. Redmer, S. Regan, and H. Sawada, J. Quant. Spectrosc. Radiat. Transf. 99, 225 (2006).

[31] G. Gregori, S. H. Glenzer, K. B. Fournier, K. M. Campbell, E. L. Dewald, O. S. Jones, J. H. Hammer, S. B. Hansen, R. J. Wallace, and O. L. Landen, Phys. Rev. Lett. 101, 045003 (2008).

[32] D. Pines, and D. Bohm, Phys. Rev., 85, 338 (1952).

[33] D. Pines, and P. Nozieres, The Theory of Quantum Fluids, Addison-Wesley, Redwood, CA, 1990.

[34] G. Zimmerman and R. More, J. Quant. Spectrosc. Radiat. Transfer 23, 517 (1980).

[35] D. D. Burgess and R. W. Lee, J. Phys. (Paris), Colloq. 43, C2-413 (1982).

[36] R. M. More, J. Quant. Spectrosc. Radiat. Transfer 27, 345 (1982).

[37] G. Ecker and W. Kröll, Phys. Fluids 6, 62 (1963).

[38] J. C. Stewart and K. D. Pyatt, Jr., Astrophys. J. 144, 1203 (1966).

[39] H. R. Griem, Plasma Spectroscopy, McGraw-Hill, New York, 1964.

[40] O. Ciricosta, S. M. Vinko, H.-K. Chung, B.-I. Cho, C. R. D. Brown, T. Burian, J. Chalupsky´, K. Engelhorn, R.W. Falcone, C. Graves, V. Ha´jkova´, A. Higginbotham, L. Juha, J. Krzywinski, H. J. Lee, M. Messerschmidt, C. D. Murphy, Y. Ping, D. S. Rackstraw, A. Scherz, W. Schlotter, S. Toleikis, J. J. Turner, L. Vysin, T. Wang, B. Wu, U. Zastrau, D. Zhu, R.W. Lee, P. Heimann, B. Nagler, and J. S. Wark., Phys. Rev. Lett. 109, 065002 (2012).

[41] J. MacFarlane, I. Golovkin, and P. Woodruff, J. Quant. Spectrosc. Radiat. Transfer 99, 381 (2006).

[42] B. J. Bloch, and L. B. Mendelsohn, Phys. Rev. A, 12, 1197 (1975).

[43] P. Eisenberger, and P. M. Platzman, Phys. Rev. A, 2, 415 (1970).

[44] R. Currat, P. D. DeCicco, and R. Kaplow, Phys. Rev. B, 3, 243 (1971).

FIGURE CAPTIONS

Figure 1 (Color online) - Previously published studies of single shock compressed CH foils. Calculated Hugoniot curve for three-shocked compressed CH capsule [9-15].

Figure 2 (Color) - Logarithmic plot of the screening function q(k), for carbon, using the Debye approximation and the complete RPA description under plasma conditions of $Z_C=4$, with n_e = (1.45, 1.35, 1.20) x 10^{24} cm^{-3} and T_e=6.5, 10, and 13.5 eV respectively.

Figure 3 (Color) - The experimental setup to study spherically convergent coalescing shocks in CH capsules; a.) Schematic diagram of the target geometry, laser beam configuration, and k-vectors; b.) Photo of CH cone- in-half-shell target; c.) 2-D Helios simulation of the mass density is shown as a function of CH shell radius, and input pulse shape dimensions (TW and time duration) along with shock conditions explained in this study.

Figure 4 (Color) - Thomson scattering curve fit analysis. Measured scattered spectra (blue) and best fit (red) to the Compton x-ray scatter features from multi-shocked CH ablators at t = 3.4 ns, 3.5 ns, 3.6 ns, and 3.8 ns, yielding n_e, T_e for $Z_C=4$.

Figure 5 (Color) - RMS fit of the full x-ray Thomson scattered spectrum (inelastic and elastic feature) for CH x-ray scattering data taken at t = 3.4 ns (400 ps after shock coalescence) indicating that single shot data from coalescing shocks provide accurate characterization with 15-20% error bar.

Figure 6 (Color) - Calculated Thomson scattering profile calculated with a.) Form Factor Approximation and b.) Impulse Approximation bound-free models for ionization states of $Z_C=2$, and $Z_C=4$.

Figure 7 (Color online) - Direct measurements of the a.) Mass density, b.) Electron temperature, and c.) Electron density, inferred from spectrally resolved x-ray Thomson scattering plotted as a function of time (using bound-free models IA and FFA). Data points are plotted with 2-D Hydrodynamic simulation (HYDRA) of multi-shocked compressed CH capsules.

FIGURES

Figure 1

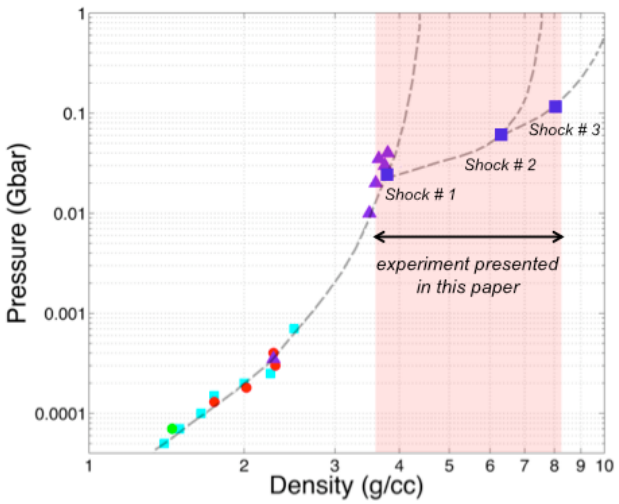

Figure 2

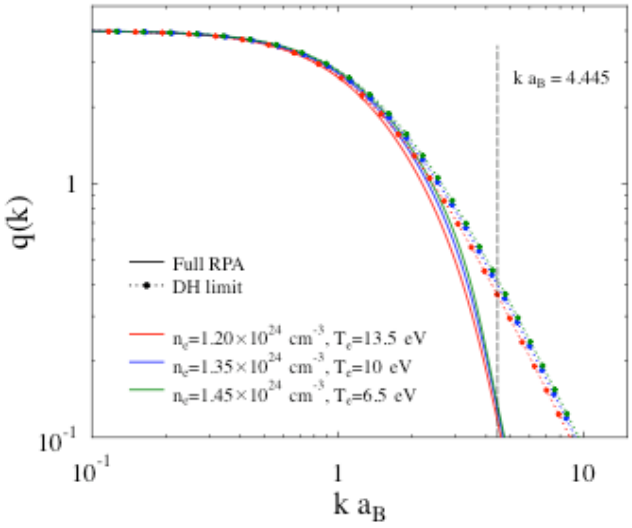

Figure 3

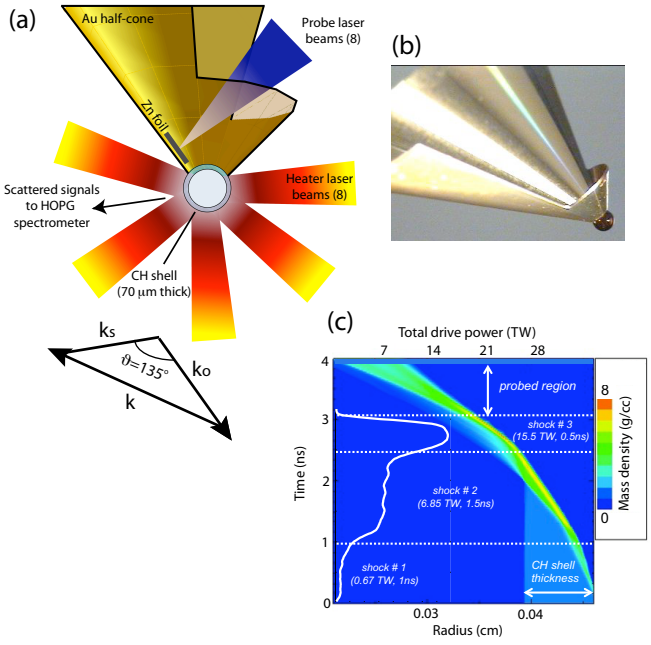

Figure 4

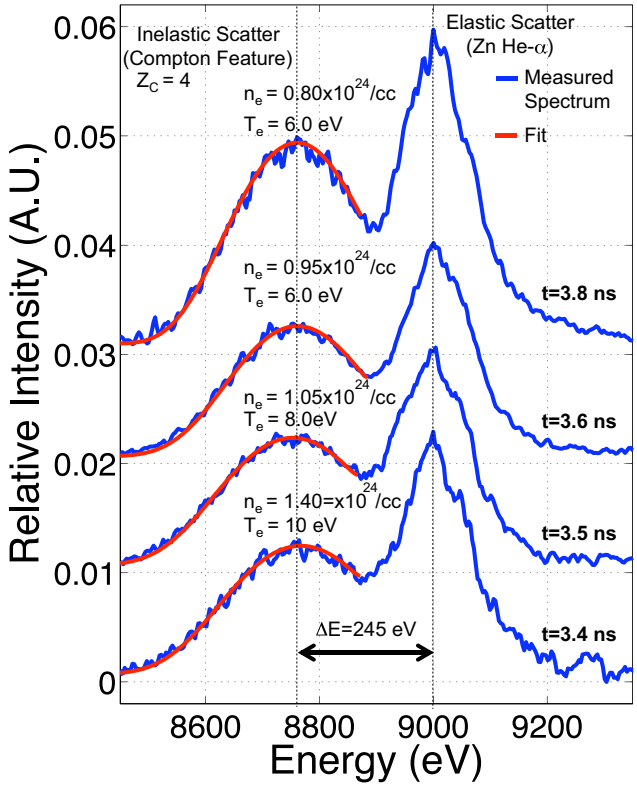

Figure 5

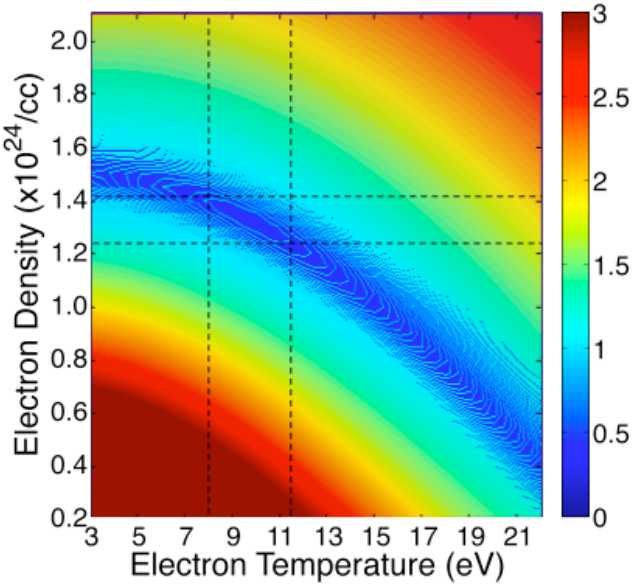

Figure 6

(a)

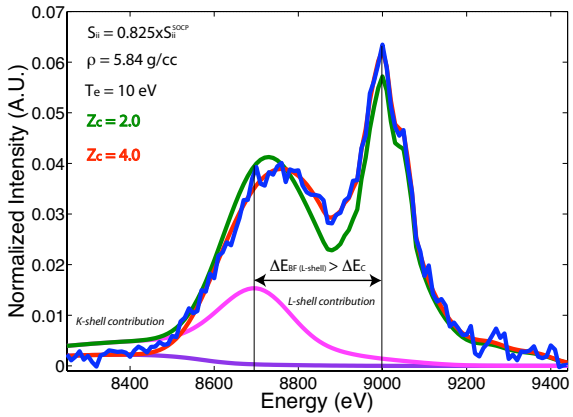

(b)

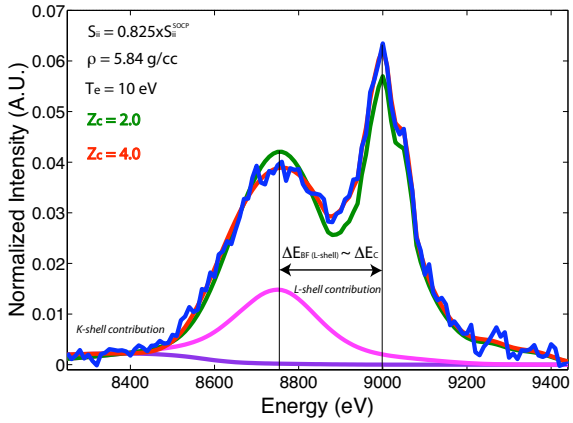

Figure 7

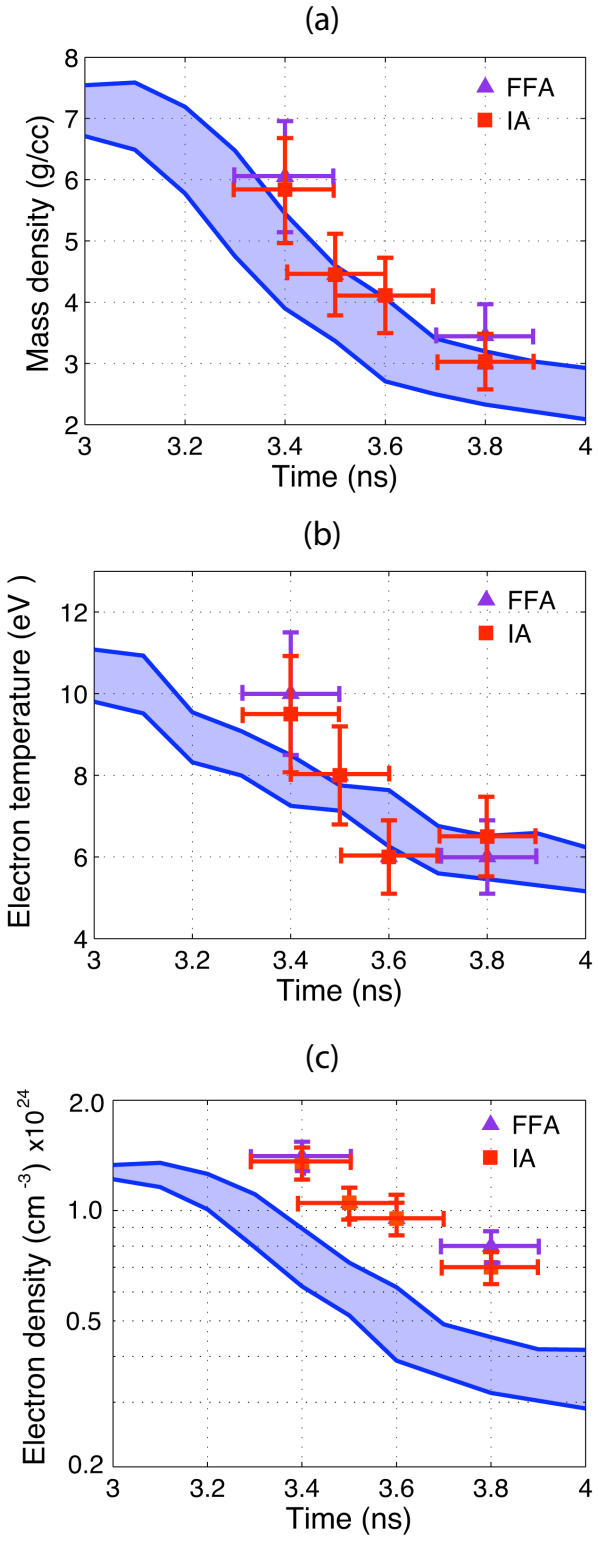
(a)
Mass density (g/cc)
Time (ns)
FFA
IA
(b)
Electron temperature (eV)
Time (ns)
FFA
IA
(c)
Electron density (cm^{-3}) x10^{24}
Time (ns)
FFA
IA